Morphogen gradients can convey position and time in growing tissues

Roman Vetter[1, 2] and Dagmar Iber[1, 2, *]

[1] *Department of Biosystems Science and Engineering, ETH Zürich, Mattenstrasse 26, 4058 Basel, Switzerland*
[2] *Swiss Institute of Bioinformatics, Mattenstrasse 26, 4058 Basel, Switzerland*

August 31, 2023

During development, cells need to make fate decisions according to their position and the developmental timepoint. Morphogen gradients provide positional information, but how timing is controlled has remained elusive. Here, we show that in morphogen gradients with constant decay length, cells experience transient, hump-shaped concentration profiles if the morphogen source expands in parallel with the uniformly growing tissue. This transient signal can convey time. We further show that opposing steady-state morphogen gradients with equal decay length, as found in the vertebrate neural tube, can synchronise cell fate decisions along the entire expanding patterning axis, because the product of the two opposing concentration gradients is constant along it. In case of an increasing amplitude, cells experience a transient hump signal, while in case of constant gradient amplitudes, the concentration product declines continuously as the tissue expands — a hallmark of a depletion timer. Once the tissue reaches a critical size and the concentrations a critical value, a cell fate switch can be triggered. Timers based on morphogen gradients offer a simple mechanism for the simultaneous control of position and time and might apply in many patterning systems, as uniform growth is observed widely in development.

Keywords: tissue patterning, morphogen gradient, time, opposing gradients, neural tube, Sonic hedgehog

1 Introduction

Morphogen gradients guide spatial patterning and cell differentiation during development. In the French flag model, concentration thresholds define the locations of domain boundaries in the tissue [1]. In addition to their relative position, cells need to track time to make the correct fate decisions [2]. A wide range of timer mechanisms have been identified [3], including organism-wide timers based on temperature, nutrition, or hormonal changes, and local timers based on intracellular oscillators, accumulation or depletion processes [4–17]. However, how processes are coordinated and synchronized across morphological fields remains largely unknown. We now show that morphogen gradients can convey not only position, but also time during development.

The development of the central nervous system (CNS) has been established as a paradigm for gradient-controlled cell differentiation [18], and we will draw on the quantitative data that has been gathered for this model system. The CNS develops from the neural tube (NT) that runs along the rostral-caudal axis of the embryo. Neural development is controlled by opposing Sonic Hedgehog (SHH) and Bone morphogenetic protein (BMP) gradients that define different progenitor domains along the dorsal-ventral (DV) axis (Fig. 1). Quantitative analysis of the mouse NT at the forelimb level revealed that cell differentiation commences about two days after the start of NT development along the entire DV axis [19]. How this timepoint is set is unknown, but it is preceded by a transient response of the SHH and BMP pathways [20–24].

SHH and BMP are secreted from the two opposite ends of the NT. The SHH gradient and the SHH reporter GBS-GFP as well as the BMP readout pSMAD have been quantified and follow an exponential function in the patterning domain between floor plate and roof plate [22, 24]. While the gradient decay lengths are constant, the SHH gradient amplitude rises continuously over time [22]. Despite this gradual increase, the response to SHH, as monitored by GBS-GFP, is a transient hump, sharply rising at first and slowly receding later on [20–22]. The mechanisms that may produce such a response are elusive [22].

By solving a reaction-diffusion model, we demonstrate that the widening of the morphogen source on the growing tissue, as has been reported for SHH in the developing NT [19], results in a gradual increase in the morphogen amplitude, resembling that reported for SHH. In case of a constant gradient decay length, as is also the case for SHH in the NT, this rising amplitude results in hump-shaped concentration profiles at fixed relative positions in the tissue. While the local concentration can convey positional information, the duration of the hump in the morphogen response can convey time. We further show that anti-parallel steady-state morphogen gradients can synchronise developmental decisions along the expanding patterning axis.

2 Results

2.1 Morphogen concentration gradient

The morphogen gradient shape can be derived by solving the appropriate reaction-diffusion equation. The measured constant characteristic length $\lambda = \sqrt{D/k}$ (where D is the morphogen diffusivity and k its turnover rate) suggests that the spatial SHH gradient is in quasi-steady state on the patterning time scale [25], despite the time-dependent amplitude. This is consistent with measurements of the Hh dynamics in the *Drosophila* wing disc, where the Hh-GFP diffusion coefficient was determined as $D_{\mathrm{Hh}} = 0.033 \pm 0.006\,\mu\mathrm{m}^2\,\mathrm{s}^{-1}$ and the Hh-GFP turnover rate as $k_{\mathrm{Hh}} = 6.7 \times 10^{-4}\,\mathrm{s}^{-1}$ [26]. The characteristic time to steady state [27], $\tau = (1 + x/\lambda)/2k_{\mathrm{Hh}} \approx 25$ minutes at $x = \lambda$, is thus short relative to the duration of NT patterning. The corresponding gradient decay length $\lambda = \sqrt{D_{\mathrm{Hh}}/k_{\mathrm{Hh}}} = 7\,\mu\mathrm{m}$ of Hh-GFP in the *Drosophila* wing disc is remarkably close to that measured for SHH-GFP, $\lambda \approx 13\,\mu\mathrm{m}$, in the mouse NT [24, 28],

*Corresponding author: dagmar.iber@bsse.ethz.ch

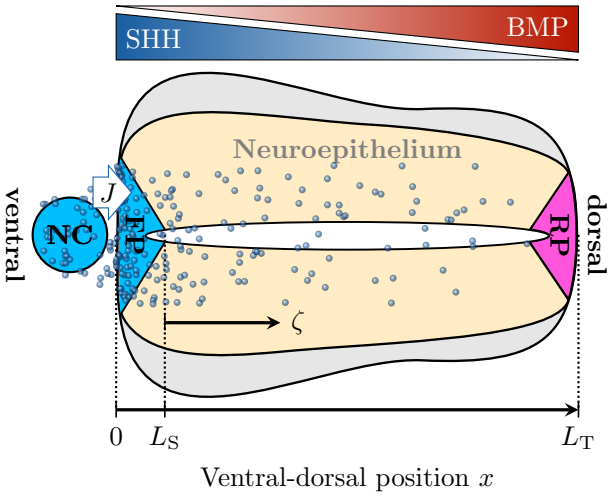

Figure 1: Patterning of the developing neural tube. Schematic cross section of the neural tube with floor plate (FP), roof plate (RP), and notochord (NC). SHH (blue molecules) is secreted from the NC and FP, and diffuses dorsally along the neuroepithelium, forming an exponential gradient. BMP is secreted from the RP, forming an anti-parallel gradient. The (positive or negative) net flux of SHH from the NC to the FP is represented by J.

and somewhat shorter than $\lambda \approx 20\,\mu\text{m}$ for untagged SHH [22]. The difference between Hh-GFP in the *Drosophila* wing disc and SHH-GFP in the mouse neural tube could be due to differences in the regulatory interactions [28, 29]. In conclusion, we will now assume that the gradient is in quasi-steady state on the growing domain.

We approximate the tissue by a 1D domain of total length L_T, with the coordinate x running from the side of the source, $x = 0$, to the other end, $x = L_T$. In case of SHH in the NT, the domain would start at the ventral limit of the floor plate (FP), and extend to the dorsal end of the roof plate (RP) (Fig. 1). The morphogen distribution along the uniformly expanding domain can then be described with a 1D steady-state reaction-diffusion equation [30]:

$$0 = pH(L_S - x) - kc(x) + D\frac{d^2c}{dx^2}(x). \tag{1}$$

Here, c denotes the morphogen concentration, p the morphogen production rate, k the turnover rate, D the diffusion coefficient, and H the Heaviside step function that restricts the morphogen production to the source of length L_S:

$$H(L_S - x) = \begin{cases} 1 & x \le L_S \\ 0 & \text{else} \end{cases}.$$

For simplicity, we will assume that the boundary far from the source is impermeable, and use a zero-flux boundary condition at $x = L_T$:

$$\frac{dc}{dx}(L_T) = 0.$$

We will show later that this assumption has little impact on the predicted gradient shape. In the first instance, we will use the same zero-flux boundary condition also at the boundary at the source, $x = 0$,

$$\frac{dc}{dx}(0) = 0.$$

However, in the NT, there is no obvious diffusion barrier at this boundary, as SHH diffuses between the adjacent SHH-secreting notochord (NC) and the FP. Accordingly, we will later also explore the impact of SHH diffusion across this boundary. Eq. 1 can be solved with basic calculus by splitting the unknown concentration profile into two domains, one containing the morphogen source, and another one in which the patterning takes place:

$$c(x) = \begin{cases} c_S(x) & 0 \le x \le L_S \\ c_P(x) & L_S \le x \le L_T \end{cases}.$$

At the interface between source and patterning domain ($x = L_S$), we require continuity in the concentration and flux:

$$c_S(L_S) = c_P(L_S) \quad \text{and} \quad \frac{dc_S}{dx}(L_S) = \frac{dc_P}{dx}(L_S).$$

With these boundary conditions, the solution for the morphogen concentration reads

$$c_S(x) = \frac{p}{k}\left(1 + \frac{\sinh\left[(L_S - L_T)/\lambda\right]}{\sinh\left[L_T/\lambda\right]}\cosh\left[\frac{x}{\lambda}\right]\right)$$
$$c_P(x) = \frac{p}{k}\frac{\sinh\left[L_S/\lambda\right]}{\sinh\left[L_T/\lambda\right]}\cosh\left[\frac{L_T - x}{\lambda}\right]$$

with decay length $\lambda = \sqrt{D/k}$.

The position where the zero-flux boundary condition is imposed opposite of the morphogen source has a negligible quantitative impact on the concentration gradient, as long as it is far away from the source ($L_T \gg L_S$), which is always the case in the NT. One can thus make an additional simplification without altering the solution in any practically measurable way. Instead of imposing $dc/dx = 0$ at $x = L_T$, we can impose it infinitely far away from the source at $x = \infty$. With this modification, the concentration simplifies to

$$c_S(x) = \frac{p}{k}\left(1 - \exp\left[-\frac{L_S}{\lambda}\right]\cosh\left[\frac{x}{\lambda}\right]\right)$$
$$c_P(x) = \frac{p}{k}\sinh\left[\frac{L_S}{\lambda}\right]\exp\left[-\frac{x}{\lambda}\right]. \tag{2}$$

The morphogen gradient amplitude c_0 at the source boundary follows as

$$c_0 = c(L_S) = \frac{p}{2k}\left(1 - \exp\left[-2\frac{L_S}{\lambda}\right]\right).$$

This concentration profile (Fig. 2A) resembles that reported for SHH in the mouse NT [22], except for the maximal amplitude

$$c_{\max} = c(0) = \frac{p}{k}\left(1 - \exp\left[-\frac{L_S}{\lambda}\right]\right), \tag{3}$$

which is located at the very start of the domain ($x = 0$) according to the model, while experiments find the peak inside the FP, near its dorsal end [22]. To address this discrepancy, we will next include SHH secretion from or into the NC ($x < 0$) and remove the diffusion barrier between NT and NC, i.e. the homogeneous Neumann boundary condition between the NC and the FP for SSH.

2.2 Morphogen flux from or to the notochord

We now generalise the reaction-diffusion model to incorporate a finite morphogen flux J in or out of the NT (Fig. 1). The boundary condition at $x = 0$ is modified to

$$-D\frac{dc}{dx}(0) = J.$$

This adds the term $(J/\lambda k)\exp[-x/\lambda]$ to the resulting concentration profile:

$$c_S(x) = \frac{p}{k}\left(1 - \exp\left[-\frac{L_S}{\lambda}\right]\cosh\left[\frac{x}{\lambda}\right] + \frac{J}{\lambda p}\exp\left[-\frac{x}{\lambda}\right]\right)$$
$$c_P(x) = \frac{p}{k}\left(\sinh\left[\frac{L_S}{\lambda}\right] + \frac{J}{\lambda p}\right)\exp\left[-\frac{x}{\lambda}\right]. \tag{4}$$

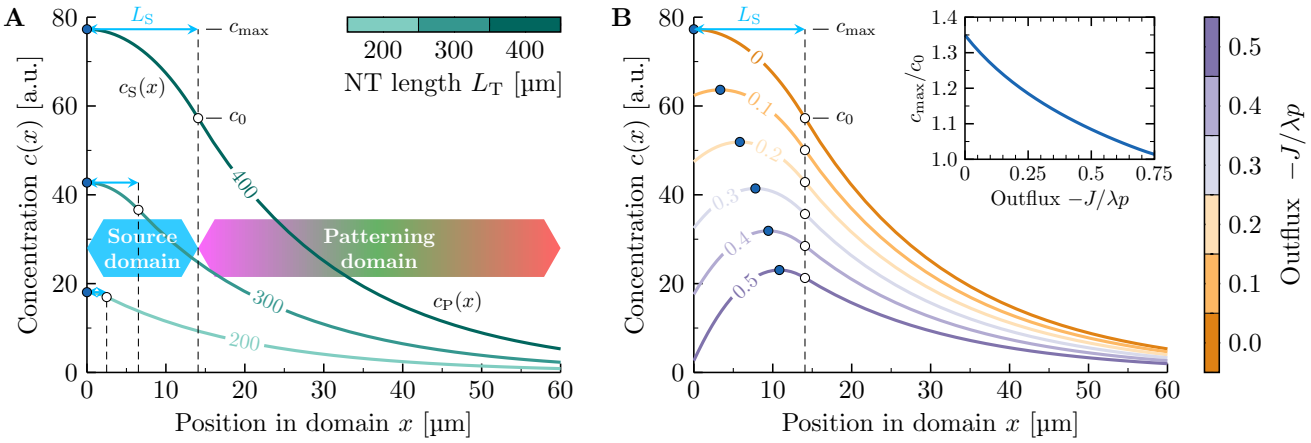

Figure 2: SHH gradient in the growing neural tube. **A**, Eq. 2 is plotted for different NT lengths using the quadratic fit $c_{max}(L_T)$ from Fig. 3A. **B**, Eq. 4 at fixed total NT length $L_T = 400\,\mu m$ for different morphogen outflux values from the FP to the NC, as labeled. Maximum concentrations c_{max} (blue dots) and boundary concentrations c_0 (white dots) are indicated. With increasing outflux, the maximum concentration approaches the source boundary amplitude: $c_{max} \to c_0$ (B, inset).

The amplitude c_0 at the source boundary then reads

$$c_0 = c(L_S) = \frac{p}{2k}\left(1 - \exp\left[-2\frac{L_S}{\lambda}\right] + \frac{2J}{\lambda p}\exp\left[-\frac{L_S}{\lambda}\right]\right).$$

For a positive influx $J > 0$, the maximum concentration still occurs at $x = 0$ and increases by $J/(\lambda k)$:

$$c_{max} = c(0) = \frac{p}{k}\left(1 - \exp\left[-\frac{L_S}{\lambda}\right] + \frac{J}{\lambda p}\right).$$

A negative flux $J < 0$ (corresponding to an outflux of SHH from the FP to the NC), on the other hand, shifts the peak concentration dorsally, to the interior of the FP (Fig. 2B). The concentration profile obtained with outflux strongly resembles the reported profiles of SHH in the NT [22] and Bicoid (Bcd) in the early *Drosophila* embryo [31]. The maximum can be found by requiring that $dc/dx = 0$. It is

$$\begin{aligned} c_{max} &= \max_{0\le x\le L_S} c(x) \\ &= \frac{p}{k}\left(1 - \sqrt{\exp\left[-2\frac{L_S}{\lambda}\right] - \frac{2J}{\lambda p}\exp\left[-\frac{L_S}{\lambda}\right]}\right). \end{aligned} \tag{5}$$

This maximum is attained at position

$$x_{max} = \arg\max_{0\le x\le L_S} c(x) = \frac{\lambda}{2}\ln\left[1 - \frac{2J}{\lambda p}\exp\left[\frac{L_S}{\lambda}\right]\right]$$

which progressively approaches the source-pattern boundary at $x = L_S$ (the dorsal FP boundary in the NT) with increasing morphogen outflux. Accordingly, the maximum concentration c_{max} approaches the exponential amplitude c_0 with increasing outflux (Fig. 2B, inset). To reduce the mathematical complexity in our further analysis below, we will therefore express the morphogen gradient in the patterning domain by

$$C(x) \approx c_{max}\exp\left[-\frac{x - L_S}{\lambda}\right], \quad x \ge L_S, \tag{6}$$

which is valid in good approximation, considering the reported shape of the Bcd and SHH profiles [22, 31]. The subsequent results are qualitatively unaffected by this simplification.

2.3 Gradient amplitude dynamics

According to Eq. 5, the gradient amplitude increases with the size of the source. The maximal SHH amplitude and the FP length have been reported for different NT lengths (Fig. 3A) [19, 21, 22]. We can now use these measurements to parameterise our model.

In previous work [22], a linear model ($n = 1$) was fitted to the maximum SHH concentrations. While this fits the data reasonably well, the fit improves for higher-order polynomial functions,

$$c_{max} = \frac{p}{k}\left[\alpha + \left(\frac{L_T}{\beta}\right)^n\right], \tag{7}$$

and is optimal for $n = 3.78 \pm 0.40$ (Fig. 3A, Table 1). Balancing Eq. 7 with Eq. 3, we can infer how the FP must expand with the NT to yield the measured increase in the SHH amplitude. The resulting relationship

$$L_S(L_T) = -\lambda\ln\left[1 - \alpha - \left(\frac{L_T}{\beta}\right)^n\right] \tag{8}$$

matches the reported FP length very well (Fig. 3B). Even though the FP expands passively with the uniformly growing domain [19], the functional relationship is non-linear because the FP is not present from the start, but is only induced by SHH from the notochord.

Note that the prefactor p/k in Eq. 7 merely sets the arbitrary concentration scale. By fitting Eq. 7 alone to measured amplitudes, the value of p/k is not uniquely defined and this prefactor can be accommodated in the values of α and β with appropriate unit adjustment. With the simultaneous fit of Eq. 8 to measured source lengths, however, one can determine optimal values for p/k, α and β uniquely. Nevertheless, p/k still only represents the arbitrary concentration scale used in the SHH amplitude data [22].

2.4 Hump-shaped gradient dynamics on growing domains

Combining Eqs. 6 and 7, the morphogen concentration can be evaluated at relative positions $\zeta = (x - L_S)/L_T$ along the patterning domain (Fig. 1), and at developmental stages of tissue growth as quantified by the total domain length L_T:

$$C(\zeta, L_T) \approx \frac{p}{k}\left[\alpha + \left(\frac{L_T}{\beta}\right)^n\right]\exp\left[-\frac{\zeta L_T}{\lambda}\right] \tag{9}$$

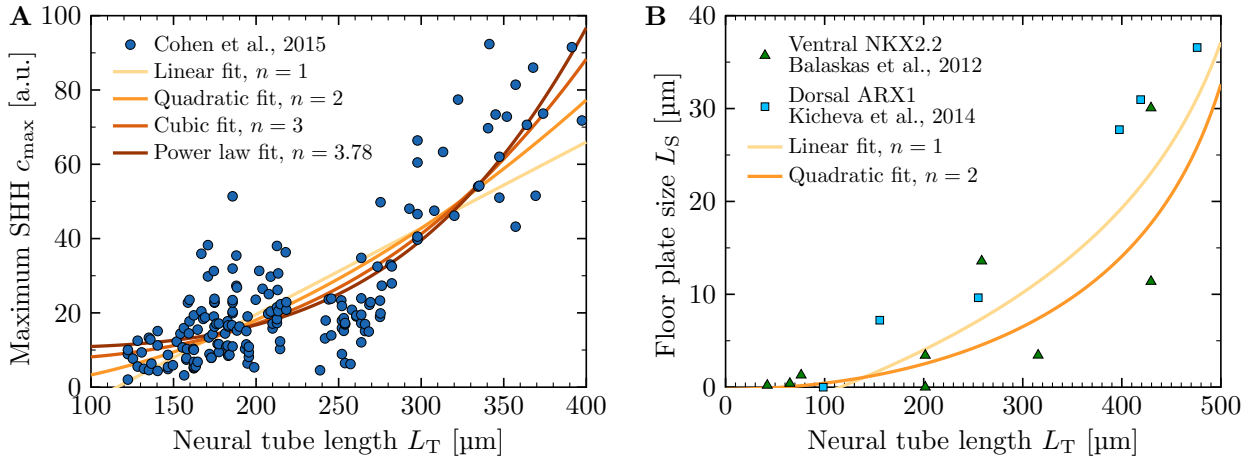

Figure 3: SHH gradient amplitude in the growing neural tube. **A**, Polynomial models (coloured lines) fitted to the increasing SHH gradient amplitude (blue dots, extracted from Ref. [22]) in the growing NT. **B**, The floor plate size inferred from the fitted maximum SHH concentration using Eq. 8 matches the reported data from Refs. [19, 21]. Developmental time was converted to NT length using the linear expansion law by Cohen et al. [22].

Table 1: SHH gradient amplitude dynamics. Parameters were obtained by least-squares fitting Eq. 7 to the data in Fig. 3A.

Model	Parameter	Unit	Value	SE	RMSE [µm]	Adjusted R^2
linear ($n = 1$)	p/k	a.u.	104.43	0.38	11.8	0.616
	α	—	−0.257	0.030		
	β	µm	450	26		
quadratic ($n = 2$)	p/k	a.u.	149.26	0.32	10.9	0.674
	α	—	−0.011	0.010		
	β	µm	550	14		
cubic ($n = 3$)	p/k	a.u.	150.1	2.6	10.3	0.706
	α	—	0.0458	0.0074		
	β	µm	490.4	7.9		
power law (n free)	p/k	a.u.	149.9	1.6	10.3	0.711
	α	—	0.070	0.012		
	β	µm	463	12		
	n	—	3.78	0.40		

At fixed ζ, the concentration first increases as the tissue expands, before it starts declining again (Fig. 4A). For the quadratic relationship ($n = 2$), the reversal point occurs earlier than for the linear model ($n = 1$) (Fig. 4B). As the NT grows linearly in time [19], the NT length where the peak morphogen concentration is attained, L_{peak}, directly relates to developmental time, allowing the SHH dynamics to be compared to the reported signalling dynamics [21, 24]. The measured SHH gradient decay length λ and amplitude (α, β, n) directly determine the NT length at which the peak $C_{\text{peak}}(\zeta) = C(\zeta, L_{\text{peak}})$ is reached at a given relative position ζ. This relationship can be found from $\partial C/\partial L_T = 0$ and it reads

$$\zeta = \frac{\lambda}{L_{\text{peak}}} \frac{n(L_{\text{peak}}/\beta)^n}{\alpha + (L_{\text{peak}}/\beta)^n}.$$

In case of the linear fit ($n = 1$), the NT length where the peak is attained follows as

$$L_{\text{peak}} = \frac{\lambda}{\zeta} - \alpha\beta \approx \frac{19.3\,\mu\text{m}}{\zeta} + 115\,\mu\text{m}. \tag{10}$$

whereas it is

$$\begin{aligned} L_{\text{peak}} &= \frac{\lambda}{\zeta} + \sqrt{\left(\frac{\lambda}{\zeta}\right)^2 - \alpha\beta^2} \\ &\approx \frac{19.3\,\mu\text{m}}{\zeta} + \sqrt{\left(\frac{19.3\,\mu\text{m}}{\zeta}\right)^2 + (58.7\,\mu\text{m})^2} \end{aligned} \tag{11}$$

for the quadratic fit ($n = 2$). The peak is thus attained earlier further away from the source (Fig. 4A,B).

The local hump corresponds to a transient activation of the SHH pathway. At fixed relative positions ζ in the patterning domain, the local morphogen concentration crosses any threshold concentration below the peak twice: Once to exceed it, and a second time at a later timepoint to drop below it again. For any threshold $\theta \in (0, 1)$, the duration of the transient activation can be determined numerically as the distance $\Delta L = L_2 - L_1$ between the two crossing points where $C(\zeta, L_1) = C(\zeta, L_2) = \theta C_{\text{peak}}(\zeta)$ (Fig. 4B). ΔL corresponds to the length of the growing domain gained over the duration of signalling. For a linearly increasing morphogen gradient amplitude ($n = 1$), it can be found by inverting Eq. 9, and it reads

$$\Delta L = \frac{\lambda}{\zeta}\left(W_0\left[-\frac{\theta}{e}\right] - W_{-1}\left[-\frac{\theta}{e}\right]\right) \tag{12}$$

independent of α and β. Here, W_k denotes the k-th branch of Lambert's W function (the product logarithm), and e is Euler's constant. The timer duration is thus inversely proportional to the relative position in the patterning domain, $\Delta L \sim \zeta^{-1}$ for $n = 1$ (Fig. 4C). For a quadratically increasing morphogen gradient amplitude ($n = 2$), it can be found numerically, and still approximately follows $\sim \lambda/\zeta$ curves (Fig. 4D). Supposing a uniform threshold θ in the domain, the transient activation of

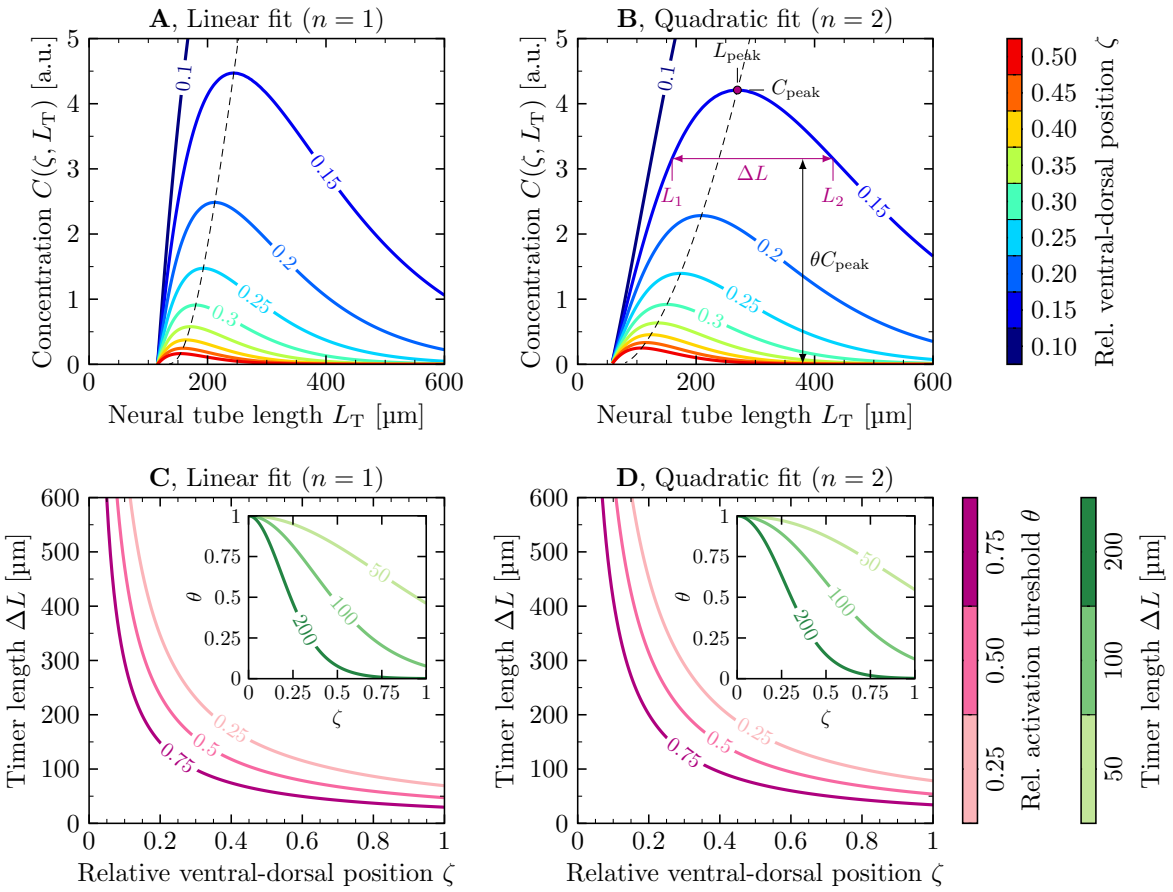

Figure 4: Transient gradient dynamics on growing domains. Time-dependent concentration at different ventral-dorsal positions ζ (colours) for a linearly increasing gradient amplitude (**A**) and a quadratically increasing gradient amplitude (**B**). Eq. 9 is plotted using the parameters from the measured SHH gradient (Table 1). The dashed lines show the evolution of the peak concentration C_{peak}, given by Eqs. 10 and 11. Duration (in terms of domain expansion ΔL over time) of the transient activation of the SHH pathway through exceedance of a fraction θ of the peak concentration, as a function of the relative position in the pattern, ζ, for a linearly increasing gradient amplitude (**C**, Eq. 12) and a quadratically increasing gradient amplitude (**D**). Insets show the inverse relationship, the activation threshold as a function of position for fixed timer lengths.

the SHH signalling pathway is thus longer close to the source and shorter further away from it. Conversely, if instead of the activation threshold θ, the timer length is to be uniform across the domain, then the activation threshold needs to drop in a nonlinear fashion with increasing distance from the source (Fig. 4C,D, insets), similarly to the French flag model for patterning in space.

We conclude that a hump-shaped local morphogen profile can arise if the morphogen gradient amplitude can be related to the patterning domain length via a polynomial function of order two or smaller. For a cubic ($n = 3$) or higher-order relationship, transient responses occur only close to the source. Further out, the concentration declines continuously. The gradient parameters directly determine the timing of the hump; there are no free parameters.

2.5 Synchronised timing by opposing morphogen gradients on growing domains

During NT development, cell fate decisions are largely synchronised along the patterning axis [19, 32, 33]. How such a synchronisation can be achieved across a large, growing morphogenetic field, and how timing is tied to developmental progress, is still largely elusive. While a single gradient can coordinate timing along the patterning axis, synchronisation would require a finely tuned distance-dependent readout threshold (Fig. 4C,D). We now show that opposing steady-state morphogen gradients with equal decay length, as found in the vertebrate neural tube, can serve as developmental timers that synchronously trigger a fate switch once the tissue reaches a critical size.

Opposing exponential gradients can be written as

$$C(x_i) = C_{0,i} \exp\left[-\frac{x_i - L_{S,i}}{\lambda}\right], \quad x_i \geq L_{S,i}, \quad i = 1, 2, \quad (13)$$

where x_i denotes the distance from the tissue boundary with the respective morphogen source. On a domain of total length L_T, $x_1 = x$ for one gradient and $x_2 = L_T - x$ for the second, anti-parallel gradient. If both gradients have an equal decay lengths λ, but possibly different amplitudes $C_{0,1}$ and $C_{0,2}$, the product of their concentrations,

$$P(L_T) = C(x)C(L_T - x), \quad (14)$$

is constant along the entire patterning axis, and declines uniformly in the growing tissue, as required for a depletion timer (Fig. 5A,B). The combined concentration of the opposing gradients can time development if the domain length L_T changes over time. The timer length is then given by the amount of tissue expansion required to let the product concentration drop below a threshold, $P = \theta C_{0,1} C_{0,2}$ (Fig. 5C):

$$\Delta L = -\lambda \ln \theta.$$

If, on the other hand, the amplitudes rise over time, as in the vertebrate NT, then the transient product concentration

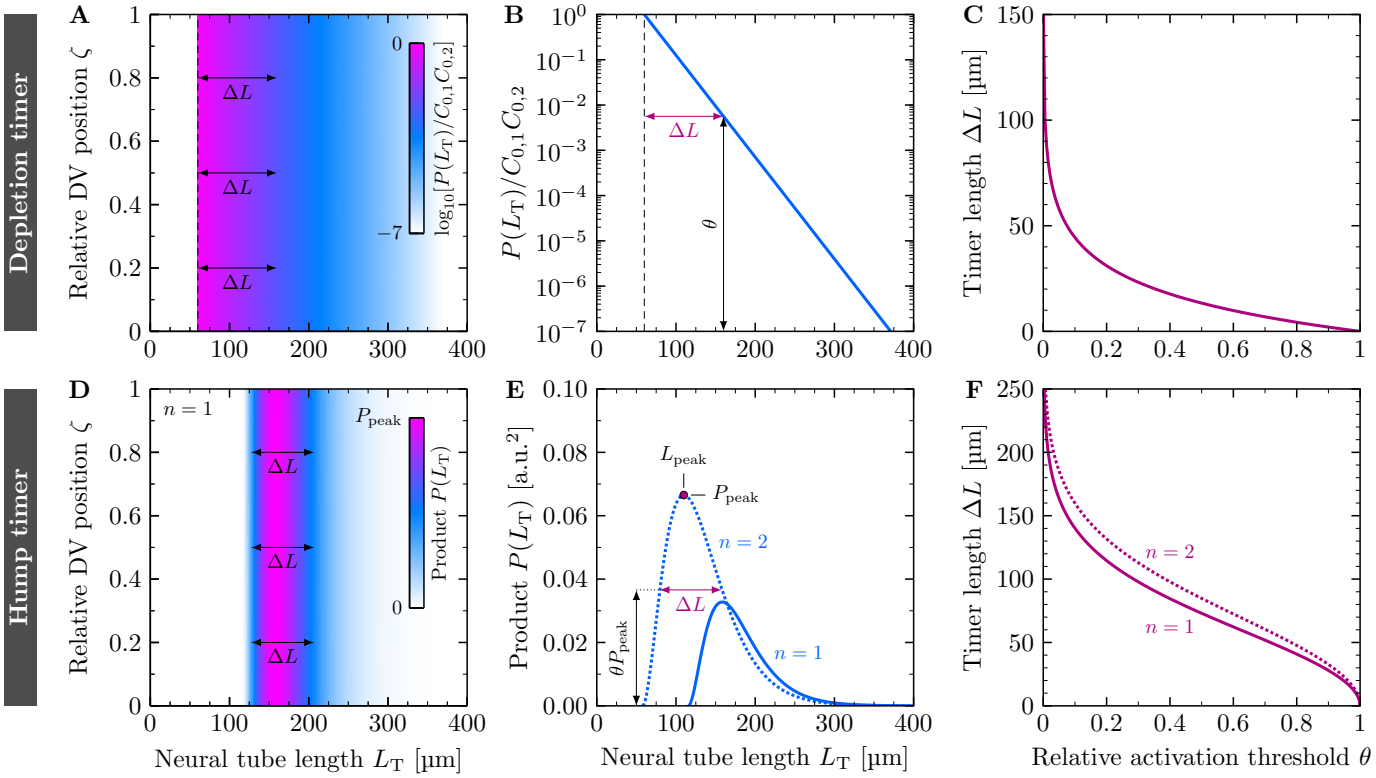

Figure 5: Synchronised timing by opposing morphogen gradients on growing domains. A, Time-dependent product of concentrations of anti-parallel morphogen gradients. Eq. 14 is plotted for fixed gradient amplitudes and source sizes, resulting in a depletion timer that is synchronous everywhere in the pattern. Note the logarithmic colour scale. **B**, The product concentration drops below a threshold (i.e., depletes) after the tissue has grown by ΔL. **C**, Length of the depletion timer as a function of the sensing threshold. **D**, Time-dependent product of concentrations of anti-parallel morphogen gradients for increasing amplitudes as measured for the SHH gradient ($n = 1$, Table 1), assuming that the opposing BMP gradient is mirror-symmetric to it. Note the linear colour scale. **E**, Time evolution of the product concentration for $n = 1, 2$, showing a transient hump as the NT lengthens over time. **F**, Length of the timer as a function of the activation threshold relative to the peak signal, as indicated in **E**.

exhibits a synchronous hump. Using the gradient amplitude fit for SHH in the mouse NT for both the SHH and the BMP gradients ($C_{0,1} = C_{0,2} = c_{max}$, Eq. 7), the peak $P_{peak} = P(L_{peak})$ occurs at a critical tissue size of $L_{peak} \approx 158\,\mu m$ for $n = 1$ and at $L_{peak} \approx 110\,\mu m$ for $n = 2$, everywhere in the patterning domain. Note that L_{peak} would be different if the amplitude of the opposing BMP gradients differed from that of the SHH gradient. Before the critical size is reached, the morphogen product increases uniformly in the entire tissue, and depletes uniformly afterwards (Fig. 5D,E). As with just one morphogen gradient, the duration of the timer with opposing gradients, measured in terms of tissue expansion ΔL, depends on the activation threshold above which the timer is turned on. The lower the threshold, the longer the timer, with uniform timer length and activation threshold across the entire pattern (Fig. 5F). Time-dependency in the amplitudes will thus affect the exact timing, but not the synchronisation along the patterning axis. All that is required for synchronisation is that both morphogen gradients have equal λ, i.e., equal D/k.

3 Discussion

We have shown that the passive expansion of the morphogen source with a uniformly expanding developing tissue results in transient, hump-like morphogen kinetics along the patterning domain. Opposing gradients with equal decay length allow for the synchronisation along the entire pattern. This new patterning paradigm offers a simple mechanism for the simultaneous control of position and timing by the morphogen gradient(s) alone. With such a mechanism, the position of progenitor domain boundaries can be controlled by the gradient amplitude and corresponding readout thresholds, while the timing of developmental processes can, in principle, be controlled with a readout of the transient nature of the concentration profiles. An expanding source and opposing gradients are found in many growing patterning systems, such that this could constitute a general timer paradigm.

A key advantage of gradient-based timers is the spatial control and alignment of cell populations over large distances. For intracellular timers, entrainment mechanisms are required to align the response of neighbouring cells [34]. In case of Notch signalling, these rely on local cell-to-cell interactions. Alternatively, the secretion of diffusible factors can coordinate local cell response, as proposed for TGF-β in hindbrain development [11]. For gradient-based timers, there is a firm bond between the rate of the gradient amplitude increase and the timing of developmental processes. As a result, spatial patterning and timing become intricately linked. The domain length at the morphogen peak is sensitive to changes in the gradient amplitude dynamics and the gradient decay length (Eqs. 10 and 11). While this may pose a challenge in the face of gradient variability and noise [24], it offers a mechanism to adjust time and length scales during evolution. Human embryos are larger than mouse embryos and develop more slowly. If the longer half-life that has been reported for the human proteome [35] translates into a larger maximal gradient amplitude (Eq. 3) and gradient decay length, the gradient-based timer mechanism will not only delay the peak of morphogen signalling in human

embryos, but will also shift it to larger domain lengths. Even if the production rate slows down in parallel to the decay rate due to a lower metabolic rate [36], a shift to longer domains would still be obtained. Gradient-based timers and those based on the local coupling of intracellular timers may thus have evolved in parallel to address different challenges in development. These are hypotheses that remain to be tested in the future.

In the mouse NT, transient SHH kinetics precede the onset of differentiation [19–22, 37, 38]. A transient response is obtained only with a linear or quadratic fit to the SHH amplitude data with a gradient-based timer, but not with the statistically favoured higher order power-law fit ($n = 3.78$, Table 1). However, due to the spread in the available SHH amplitude and FP length data (Fig. 3), the optimality of $n = 3.78$ is likely not statistically robust, and growth laws other than the power law used here could be similarly adequate. Given the technical challenges in measuring SHH gradients and FP lengths in the NT, the measured SHH amplitude and/or FP length data could be inaccurate [30]. We note that a timer based on the measured SHH gradient yields a transient response that is much slower and delayed compared to the measured kinetics of the SHH pathway [21, 22]. To achieve the same duration along the patterning axis, the readout threshold, θ, would need to decline with distance from the source (Fig. 4C,D). However, also in this case, the peak would still be reached too late close to the source (Fig. 4A,B). A timer based on the opposing SHH and BMP gradients would allow for the synchronisation of cell differentiation along the entire patterning axis with a single readout threshold at a NT length consistent with the observed onset of differentiation.

A transient activation of the SHH pathway is observed also in cultured neural stem cells, and when the SHH pathway is stimulated permanently [11, 22, 35]. Models that include both diffusible morphogens and intracellular regulatory networks will be important to understand how tissues exploit their specific advantages to robustly coordinate cell fate decisions in space and time — and to what extent they are redundant. Important biological processes are often controlled by redundant mechanisms [39], a prominent example being hindbrain development. While TGF-β terminates the SHH response and thereby controls the concomitant switch in cell differentiation from motor neurons to serotonergic neurons (5HTN), the SHH response still terminates in the absence of TGF-β signalling, albeit somewhat delayed [11, 40].

Many developmental domains expand uniformly, with the morphogen source expanding in parallel with the patterning domain, but so far only few have been analysed quantitatively [18]. In case of the Bicoid gradient in the *Drosophila* blastoderm, growth terminates before Bcd-dependent patterning [41] such that our novel timer paradigm cannot apply to the Bcd gradient. In case of Decapentaplegic (Dpp) in the *Drosophila* wing disc, not only the source, but also the gradient length λ, increases with the growing domain [42]. This gradient behaviour can be accounted to the pre-steady-state expansion of the gradient [25]. The combination of an increase in both the gradient amplitude and length results in a gradually rising concentration near the source, a decline at a distance, and a constant concentration at the level of the Dpp readout boundaries for *sal* and *dad*. While this enables the scaling of the Dpp readout positions on the growing domain [25, 43], it precludes the use of the Dpp gradient as timer.

As technological advances enable the quantitative characterisation of an increasing number of developmental systems, examples of this novel timer paradigm might be uncovered in near future. Gradient-based timers present a promising strategy also in synthetic bioengineering efforts to control position and time simultaneously.

References

[1] L. Wolpert. Positional information and the spatial pattern of cellular differentiation. *J. Theor. Biol.*, 25:1–47, 1969.

[2] M. Ebisuya and J. Briscoe. What does time mean in development? *Development*, 145, 2018.

[3] L. Busby and B. Steventon. Tissue tectonics and the multiscale regulation of developmental timing. *Interface Focus*, 11:20200057, 2021.

[4] M. Boehm and F. Slack. A developmental timing microrna and its target regulate life span in c. elegans. *Science*, 310(5756):1954–7, 2005.

[5] C. Collart, G. E. Allen, C. R. Bradshaw, J. C. Smith, and P. Zegerman. Titration of four replication factors is essential for the xenopus laevis midblastula transition. *Science*, 341(6148):893–896, 2013.

[6] K. F. Rewitz, N. Yamanaka, and M. B. O'Connor. Developmental checkpoints and feedback circuits time insect maturation. *Curr Top Dev Biol*, 103:1–33, 2013.

[7] M. Goodfellow, N. Phillips, C. Manning, T. Galla, and N. Papalopulu. microRNA input into a neural ultradian oscillator controls emergence and timing of alternative cell states. *Nat. Commun.*, 5:3399, 2014.

[8] I. Averbukh, S. L. Lai, C. Q. Doe, and N. Barkai. A repressor-decay timer for robust temporal patterning in embryonic drosophila neuroblast lineages. *Elife*, 7, 2018.

[9] J. Pickering, C. A. Rich, H. Stainton, C. Aceituno, K. Chinnaiya, P. Saiz-Lopez, M. A. Ros, and M. Towers. An intrinsic cell cycle timer terminates limb bud outgrowth. *eLife*, 7:e37429, 2018.

[10] I. Holguera and C. Desplan. Neuronal specification in space and time. *Science*, 362:176–180, 2018.

[11] J. M. Dias, Z. Alekseenko, A. Jeggari, M. Boareto, J. Vollmer, M. Kozhevnikova, H. Wang, M. P. Matise, A. Alexeyenko, D. Iber, and J. Ericson. A Shh/Gli-driven three-node timer motif controls temporal identity and fate of neural stem cells. *Sci. Adv.*, 6, 2020.

[12] S. Jain, Y. Lin, Y. Z. Kurmangaliyev, J. Valdes-Aleman, S. A. LoCascio, P. Mirshahidi, B. Parrington, and S. L. Zipursky. A global timing mechanism regulates cell-type-specific wiring programmes. *Nature*, 603:112–118, 2022.

[13] N. Konstantinides, I. Holguera, A. M. Rossi, A. Escobar, L. Dudragne, Y.-C. Chen, T. N. Tran, A. M. Martínez Jaimes, M. N. Özel, F. Simon, Z. Shao, N. M. Tsankova, J. F. Fullard, U. Walldorf, P. Roussos, and C. Desplan. A complete temporal transcription factor series in the fly visual system. *Nature*, 604:316–322, 2022.

[14] E. Clark, M. Battistara, and M. A. Benton. A timer gene network is spatially regulated by the terminal system in the *Drosophila* embryo. *eLife*, 11:e78902, 2022.

[15] M. Son, T. Frank, T. Holst-Hansen, A. G. Wang, M. Junkin, S. S. Kashaf, A. Trusina, and S. Tay. Spatiotemporal NF-κB dynamics encodes the position, amplitude and duration of local immune inputs. *Sci. Adv.*, 8:eabn6240, 2022.

[16] X. Soto, J. Burton, C. S. Manning, T. Minchington, R. Lea, J. Lee, J. Kursawe, M. Rattray, and N. Papalopulu. Sequential and additive expression of mir-9 precursors control timing of neurogenesis. *Development*, 149:dev200474, 2022.

[17] E. Camacho-Aguilar, S. Yoon, M. A. Ortiz-Salazar, and A. Warmflash. Combinatorial interpretation of BMP and WNT allows BMP to act as a morphogen in time but not in concentration. *bioRxiv*, 2023.

[18] J. Briscoe and S. Small. Morphogen rules: design principles of gradient-mediated embryo patterning. *Development*, 142:3996–4009, 2015.

[19] A. Kicheva, T. Bollenbach, A. Ribeiro, H. P. Valle, R. Lovell-Badge, V. Episkopou, and J. Briscoe. Coordination of

progenitor specification and growth in mouse and chick spinal cord. *Science*, 345:1254927, 2014.

[20] E. Dessaud, L. L. Yang, K. Hill, B. Cox, F. Ulloa, A. Ribeiro, A. Mynett, B. G. Novitch, and J. Briscoe. Interpretation of the sonic hedgehog morphogen gradient by a temporal adaptation mechanism. *Nature*, 450:717–720, 2007.

[21] N. Balaskas, A. Ribeiro, J. Panovska, E. Dessaud, N. Sasai, K. M. Page, J. Briscoe, and V. Ribes. Gene Regulatory Logic for Reading the Sonic Hedgehog Signaling Gradient in the Vertebrate Neural Tube. *Cell*, 148:273–284, 2012.

[22] M. Cohen, A. Kicheva, A. Ribeiro, R. Blassberg, K. M. Page, C. P. Barnes, and J. Briscoe. Ptch1 and Gli regulate Shh signalling dynamics via multiple mechanisms. *Nat. Commun.*, 6:6709, 2015.

[23] S. Tozer, G. Le Dréau, E. Marti, and J. Briscoe. Temporal control of BMP signalling determines neuronal subtype identity in the dorsal neural tube. *Development*, 140:1467–1474, 2013.

[24] M. Zagorski, Y. Tabata, N. Brandenberg, M. P. Lutolf, G. Tkačik, T. Bollenbach, J. Briscoe, and A. Kicheva. Decoding of position in the developing neural tube from antiparallel morphogen gradients. *Science*, 356:1379–1383, 2017.

[25] P. Fried and D. Iber. Dynamic scaling of morphogen gradients on growing domains. *Nat. Commun.*, 5:5077, 2014.

[26] P. Fried, M. Sánchez-Aragón, D. Aguilar-Hidalgo, B. Lehtinen, F. Casares, and D. Iber. A Model of the Spatio-temporal Dynamics of *Drosophila* Eye Disc Development. *PLOS Comput. Biol.*, 12:e1005052, 2016.

[27] A. M. Berezhkovskii, C. Sample, and S. Y. Shvartsman. How Long Does It Take to Establish a Morphogen Gradient? *Biophys. J.*, 99:L59–L61, 2010.

[28] C. E. Chamberlain, J. Jeong, C. Guo, B. L. Allen, and A. P. McMahon. Notochord-derived Shh concentrates in close association with the apically positioned basal body in neural target cells and forms a dynamic gradient during neural patterning. *Development*, 135:1097–1106, 2008.

[29] M. Nahmad and A. Stathopoulos. Dynamic Interpretation of Hedgehog Signaling in the *Drosophila* Wing Disc. *PLoS Biol.*, 7:e1000202, 2009.

[30] R. Vetter and D. Iber. Precision of morphogen gradients in neural tube development. *Nat. Commun.*, 13:1145, 2022.

[31] B. Houchmandzadeh, E. Wieschaus, and S. Leibler. Establishment of developmental precision and proportions in the early *Drosophila* embryo. *Nature*, 415:798–802, 2002.

[32] A. Sagner, Z. B. Gaber, J. Delile, J. H. Kong, D. L. Rousso, C. A. Pearson, S. E. Weicksel, M. Melchionda, S. N. Mousavy Gharavy, J. Briscoe, and B. G. Novitch. Olig2 and Hes regulatory dynamics during motor neuron differentiation revealed by single cell transcriptomics. *PLOS Biol.*, 16:e2003127, 2018.

[33] J. Delile, T. Rayon, M. Melchionda, A. Edwards, J. Briscoe, and A. Sagner. Single cell transcriptomics reveals spatial and temporal dynamics of gene expression in the developing mouse spinal cord. *Development*, 146, 2019.

[34] T. Tomka, D. Iber, and M. Boareto. Travelling waves in somitogenesis: Collective cellular properties emerge from time-delayed juxtacrine oscillation coupling. *Prog. Biophys. Mol. Biol.*, 137:76–87, 2018.

[35] T. Rayon, D. Stamataki, R. Perez-Carrasco, L. Garcia-Perez, C. Barrington, M. Melchionda, K. Exelby, J. Lazaro, V. L. J. Tybulewicz, E. M. C. Fisher, and J. Briscoe. Species-specific pace of development is associated with differences in protein stability. *Science*, 369:eaba7667, 2020.

[36] M. Diaz-Cuadros, O. S. Miettinen, Skinner, T. P., D. Sheedy, C. M. Díaz-García, S. Gapon, A. Hubaud, G. Yellen, S. R. Manalis, W. Oldham, and O. Pourquié. Metabolic regulation of species-specific developmental rates. *Nature*, 613:550–557, 2023.

[37] M. Saade, I. Gutiérrez-Vallejo, G. Le Dréau, M. A. Rabadán, D. G. Miguez, J. Buceta, and E. Marti. Sonic Hedgehog Signaling Switches the Mode of Division in the Developing Nervous System. *Cell Rep.*, 4:492–503, 2013.

[38] M. Saade, E. Gonzalez-Gobartt, R. Escalona, S. Usieto, and E. Martí. Shh-mediated centrosomal recruitment of PKA promotes symmetric proliferative neuroepithelial cell division. *Nat. Cell Biol.*, 19:493–503, 2017.

[39] M. A. Nowak, M. C. Boerlijst, J. Cooke, and J. M. Smith. Evolution of genetic redundancy. *Nature*, 388:167–171, 1997.

[40] J. M. Dias, Z. Alekseenko, J. M. Applequist, and J. Ericson. Tgfβ signaling regulates temporal neurogenesis and potency of neural stem cells in the CNS. *Neuron*, 84:927–939, 2014.

[41] F. He, C. Wei, H. Wu, D. Cheung, R. Jiao, and J. Ma. Fundamental origins and limits for scaling a maternal morphogen gradient. *Nat. Commun.*, 6:6679, 2015.

[42] O. Wartlick, P. Mumcu, A. Kicheva, T. Bittig, C. Seum, F. Jülicher, and M. González-Gaitán. Dynamics of Dpp Signaling and Proliferation Control. *Science*, 331:1154–1159, 2011.

[43] P. Fried and D. Iber. Read-Out of Dynamic Morphogen Gradients on Growing Domains. *PLOS ONE*, 10:e0143226, 2015.

Acknowledgements

We thank Marius Almanstötter, Marcelo Boareto, James Briscoe, José Dias, Johan Ericson, Anna Kicheva for discussions. This work was partially funded by the Swiss National Science Foundation through Sinergia grant CRSII5_170930 to DI.

Competing Interests

The authors declare that they have no competing interests.

Author Contributions

DI conceived the study and discovered the gradient-based timer. RV and DI developed the theory, analysed the data, and wrote the manuscript. RV created the figures.